JACS
JOURNAL OF THE AMERICAN CHEMICAL SOCIETY
Article
Cite This: J. Am. Chem. Soc. 2018, 140, 14627−14637
pubs.acs.org/JACS

Controlling Anisotropic Growth of Colloidal ZnSe Nanostructures

Jiajia Ning,[†,‡] Jing Liu,[§,⊥] Yael Levi-Kalisman,[‡,∥] Anatoly I. Frenkel,[*,§,¶] and Uri Banin[*,†,‡]

[†]Institute of Chemistry, The Hebrew University of Jerusalem, Jerusalem 91904, Israel
[‡]The Center for Nanoscience and Nanotechnology, The Hebrew University of Jerusalem, Jerusalem 91904, Israel
[§]Department of Materials Science and Chemical Engineering, Stony Brook University, Stony Brook, New York 11794, United States
[⊥]Department of Physics, Manhattan College, Riverdale, New York 10471, United States
[∥]Institute of Life Sciences, The Hebrew University of Jerusalem, Jerusalem 91904, Israel
[¶]Department of Chemistry, Brookhaven National Laboratory, Upton, New York 11973, United States

Supporting Information

ABSTRACT: Semiconductor nanocrystals serve as outstanding model systems for studying quantum confined size and shape effects. Shape control is an important knob for controlling their properties but so far it has been well developed mainly for heavy-metal containing semiconductor nanocrystals, limiting their further widespread utilization. Herein, we report a synthesis of heavy-metal free ZnSe nanocrystals with shape and size control through utilization of well-defined molecular clusters. In this approach, ZnSe nanowires are synthesized and their length and shape control is achieved by introduction of controlled amounts of molecular clusters. As a result of $[Zn_4(SPh)_{10}](Me_4N)_2$ clusters (Zn_4 clusters) addition, short ZnSe nanorods or ZnSe nanodots can be obtained through tuning the ratio of Zn_4 clusters to ZnSe. A study using transmission electron microscopy revealed the formation of a hybrid inorganic−organic nanowire, whereby the ligands form a template for self-assembly of ZnSe magic size clusters. The hybrid nanowire template becomes shorter and eventually disappears upon increasing amount of Zn_4 clusters in the reaction. The generality of the method is demonstrated by using isostructural $[Cu_4(SPh)_6](Me_4N)_2$ clusters, which presented a new approach to Cu doped ZnSe nanocrystals and provided also a unique opportunity to employ X-ray absorption fine structure spectroscopy for deciphering the changes in the local atomic-scale environment of the clusters and explaining their role in the process of the nanorods formation. Overall, the introduction of molecular clusters presented here opens a path for growth of colloidal semiconductor nanorods, expanding the palette of materials selection with obvious implications for optoelectronic and biomedical applications.

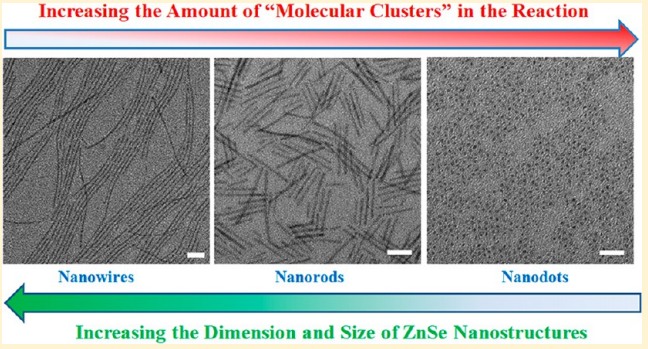

INTRODUCTION

In the past three decades, the effects of size and shape on the properties of semiconductor nanocrystals (SC NCs) were extensively studied.[1] For example, the emission from zero-dimensional (0D) spherical nanodots (NDs) is isotropic, whereas one-dimensional (1D) nanorods (NRs) and nanowires (NWs) exhibit polarized fluorescence emission.[2−4] Because of such unique size and shape dependent physical and chemical properties, SC NCs have already been widely used in many fields. In particular, SC NCs are utilized now in commercial displays providing highly improved color quality and energy saving characteristics.[5−7] The narrow tunable emission peaks along with broad excitation wavelength range can also provide multiple fluorescence signatures simultaneously for biomedical applications.[8,9] Further applications in photodetectors and solar energy harvesting are also of interest.[10,11]

The most highly developed SC NCs contain heavy-metal. In particular, for visible range applications, Cd-chalcogenide NCs reached a high level of control, and for near-infrared range (NIR) active NCs, Pb- and Hg- chalcogenide NCs have been optimized. For example, the shape of CdSe NCs can be controlled yielding 0D quantum dots, 1D rods, two-dimensional (2D) platelets and branched multipod NCs.[12−16] However, potential toxicity and regulatory restrictions related to heavy-metal elements limit their wider-spread implementation calling for development of heavy metal free SC NCs with similar high level performance. Such expansion of the palette of well-controlled semiconductor nanocrystals is of great interest also from the fundamental aspects of materials synthesis.

ZnSe is a representative of heavy-metal free and "Green" Zn-chalcogenide semiconductor materials. The ZnSe band gap in bulk material is ∼2.7 eV.[17] Because of the quantum confinement effect, ZnSe NCs could be tuned to emit in the ultraviolet (UV)

Received: June 6, 2018
Published: August 30, 2018

DOI: 10.1021/jacs.8b05941
J. Am. Chem. Soc. 2018, 140, 14627−14637

to the blue spectral range, which at present lacks in optimal SC NC based emitters.[18] Unlike cadmium chalcogenide NCs, the synthesis of high-quality ZnSe NCs is still an open challenge in nanocrystal chemistry. Until now, the research on ZnSe NCs was focused on growth of a ZnS shell on spherical ZnSe NCs to improve the fluorescence emission.[19] Impurities, such as Mn, were also introduced into ZnSe NCs to extend the fluorescence emission range.[20]

In terms of shape-control, a few effective approaches have been developed to synthesize SC NCs with different structures such as NWs, NRs or nanoplatelets.[21,22] However, it is challenging to synthesize length-controlled semiconductor NWs or NRs. In the case of ZnSe, mostly NWs were synthesized to date employing attachment of small ZnSe NCs.[23−26] Recently, 1D ZnSe NRs or rod-couples were synthesized starting with ZnSe NWs.[27,28] The ZnSe NWs were formed at first via attachment of small ZnSe dots. ZnSe NRs could be produced via ripening of ZnSe NWs after cleaning the excess precursors. Rod-couples, with two ZnSe NRs connected in a unique manner, were also prepared and their formation mechanism was investigated.[27] Additionally, Pradhan and co-workers found that Mn-doped ZnSe NRs could be synthesized via ripening ZnSe NWs with Mn impurities introduced on their surface.[29] Nonetheless, additional approaches for length- and shape-controlled nanocrystals are needed, as are new ways of introducing dopants into these NCs.

Herein, we developed a novel colloidal route to synthesize ZnSe NCs with controlled shape and size. Typically, ZnSe NWs with length of hundreds of nanometer can be synthesized in a hybrid NW template formed by self-assembly of ZnSe magic size clusters (MSCs) with oleylamine (OLA) ligand. By introducing the use of molecular clusters $[Zn_4(SPh)_{10}](Me_4N)_2$ (Zn_4 clusters) as additional reagents, we succeeded in producing length controlled ZnSe NRs, or NDs. The investigation of the growth mechanism of the ZnSe NRs shows that the added Zn_4 clusters have an important influence on the assembly of ZnSe MSCs to hybrid inorganic organic nanowire template. The isostructured $[Cu_4(SPh)_6](Me_4N)_2$ clusters (Cu_4 clusters) were also used in the synthesis. This provides a route for Cu doped ZnSe NCs. Furthermore, Cu_4 clusters offer an important characterization advantage enabling utilization of X-ray absorption fine structure (XAFS) spectroscopy to detect the evolution of the clusters in the synthesis. We also found that the thiophenol ligands on the cluster surface play a role in the length control of the hybrid template. Using MSCs along with molecular clusters is a versatile tool to synthesize SC NCs with shape and size control, applicable to additional semiconductor materials. It also provides a unique route for doping with suitable elements by tuning the type and composition of the added molecular clusters.

EXPERIMENTAL SECTION

Chemicals. Diethylzinc solution (1.0 M in hexanes), diphenylphosphine (DPP, 98%), $Zn(NO_3)_2{\cdot}6H_2O$ (99%), $Cu(NO_3)_2{\cdot}3H_2O$ (99%−104%), 1-octadecene (ODE, 90%), thiophenol (SPh) (>98%), triethylamine (>99%), tetramethylammonium chloride (TMACl, ≥98%), acetonitrile (99.8%), toluene (99%, anhydrous), hexane (95%, anhydrous), ethanol (99.8%, anhydrous), and dimethylformamide (DMF) were purchased from Sigma-Aldrich. Selenium powder (99.999%) was purchased from Strem Chemicals. Oleylamine (OLA, approximate C18 content 80−90%) was purchased from Acros.

Synthesis of $[Zn_4(SPh)_{10}](Me_4N)_2$.[30] $[Zn_4(SPh)_{10}](Me_4N)_2$ was synthesized by combining a solution of (9 g, 30 mmol) $Zn(NO_3)_2{\cdot}6H_2O$ in 70 mL of methanol to a stirred room-temperature solution of (22.8 g, 207 mmol) thiophenol and (20.9 g, 207 mmol) triethylamine in 40 mL of methanol. To this mixture was added a solution of (7.5 g, 68 mmol) tetramethylamonium chloride (TMACl) in 40 mL of methanol, and the product was then allowed to crystallize at 0 °C. The colorless crystalline product was washed with methanol and vacuum-dried.

Synthesis of $[Cu_4(SPh)_6](Me_4N)_2$.[31] $[Cu_4(SPh)_6](Me_4N)_2$ was synthesized by combining a solution of (16.4 g, 68 mmol) $Cu(NO_3)_2{\cdot}3H_2O$ in 70 mL of methanol to a stirred room-temperature solution of (20.0 g, 182 mmol) thiophenol and (18.5 g, 182 mmol) triethylamine in 40 mL of methanol. To this mixture was added a solution of (8.4 g, 77 mmol) tetramethylamonium chloride (TMACl) in 40 mL of methanol, and the product was then allowed to crystallize at 0 °C, producing a yellow solid. The solution was filtered, washed with cold methanol, and vacuum-dried.

Synthesis of Diphenylphosphine Selenium (DPP-Se).[32] Diphenylphosphine (1.85 mL, 10 mmol), toluene (15 mL), and selenium powder (78.9 mg, 10 mmol) were added into a three-necked flask under in the glovebox, and the mixture was stirred at room temperature for overnight. The solution turned clear during the reaction. Recrystallization can be afforded through addition of a minimum amount of toluene and heated to just under reflux. Crystals appear after slowly cooling to room temperature and leaving still overnight at 4 °C.

The below experiments were carried out using standard airless techniques: a vacuum/dry Ar gas Schleck line was used for synthesis.

Synthesis of ZnSe MSCs. The OLA (3 mL) and ODE (5 mL) solution was degassed and heated to 110 °C in three neck flask, and the mixture solution was kept at 110 °C with vacuum for 1 h to remove any water in the system. Then the OLA and ODE solution was cooled down to room temperature. At room temperature, diethylzinc-hexane solution (1 M, 1 mL), DMF (1 mL), and DPPSe-toluene solution (1 M, 1 mL) were injected into the three neck flask with OLA and ODE solution. Then, the mixture solution was heated slowly to 60 °C. And the reaction solution was kept at 60 °C for 48 h to grow ZnSe MSCs.

Synthesis of ZnSe NWs. After synthesis of ZnSe MSCs, the ZnSe MSCs with OLA and ODE solution was heated to 240 °C with 10 °C/min. The reaction was kept at 240 °C for 4 h to synthesis of ZnSe NWs.

Synthesis of ZnSe NCs with Shape and Size Control. After synthesis of ZnSe MSCs, the ZnSe MSCs with OLA and ODE reaction solution was used as stock solution. At 60 °C, we added Zn_4 cluster ($[Zn_4(SPh)_{10}](Me_4N)_2$)-DMF solution (1 mL DMF with different amount of Zn_4 cluster) into the ZnSe MSCs stock solution. The mixture solution was kept at 60 °C and stirred for 4 h. Then, we heated the mixture solution to 240 °C with 10 °C/min. The reaction was kept at 240 °C for a few hours to synthesis of ZnSe NRs. The synthesized ZnSe NRs can be continued to heat to 280 °C and the reaction was kept at 280 °C for 1 h to repining ZnSe NRs to increase the diameter of ZnSe NRs.

Purification of ZnSe NCs. The crude ZnSe NCs product solution was dissolved in toluene, and the NCs were precipitated by adding ethanol with the aid of centrifugation. All of ZnSe NCs products were purified with toluene and ethanol for three times.

Sample Characterizations. UV−vis absorption spectroscopy was performed on a JASCO V-570 spectrometer using quartz cuvettes. The samples were dissolved in hexane.

Fluorescence emission was performed with a Varian Cary Eclipse fluorimeter using quartz cuvettes. The samples were dissolved in hexane.

Powder X-ray diffraction (XRD) patterns were obtained using Cu Kα photons from a Phillips PW1830/40 diffractometer operated at 40 kV and 30 mA. Each sample was deposited as a thin layer on a low background-scattering quartz substrate.

Transmission electron microscopy (TEM) was performed using a FEI Tecnai G2 Spirit Twin T-12 transmission electron microscope with a LaB_6 filament running at an accelerating voltage of 120 kV. TEM grids were prepared by depositing one drop of a solution of purified nanoparticles onto an ultrathin carbon-coated grid.

Cryogenic transmission electron microscopy (cryo-TEM) enables direct imaging of assemblies of amphiphilic polymers in aqueous environments. Cryo-TEM sample preparation and imaging: a 3 μL drop

DOI: 10.1021/jacs.8b05941
J. Am. Chem. Soc. 2018, 140, 14627−14637

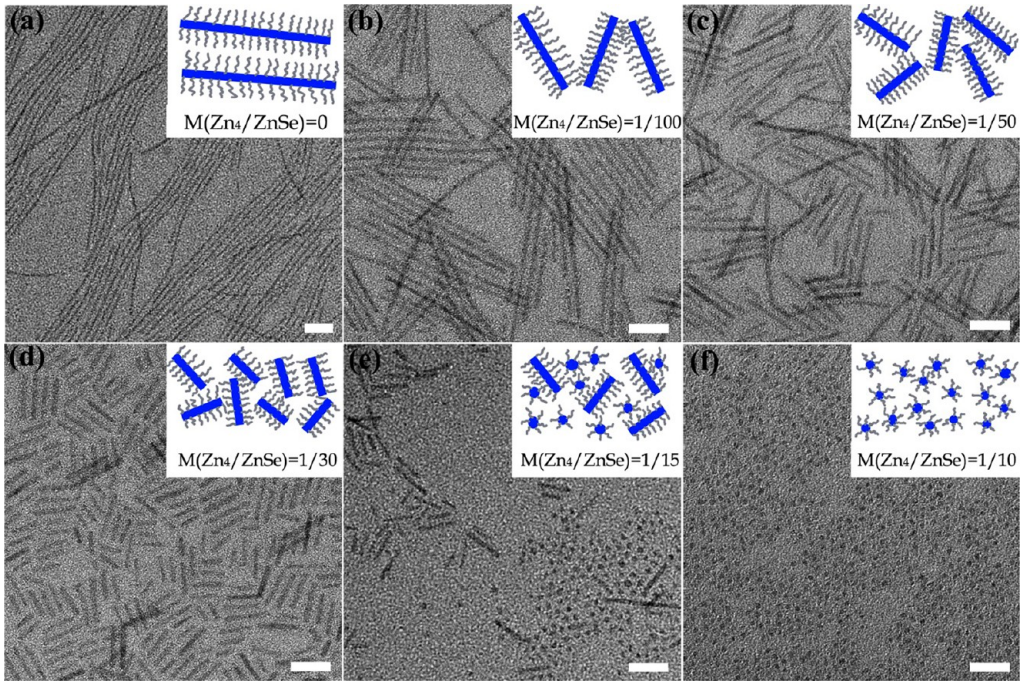

Figure 1. TEM images of ZnSe NCs synthesized at 240 °C for 4 h with different amount of Zn_4 clusters. (a) NWs synthesized without Zn_4 clusters; (b) NRs with length of ∼60 nm synthesized with Zn_4 clusters of M(Zn_4/ZnSe) = 1/100 (M being the molar ratio of Zn_4/ZnSe). (c) NRs with length of ∼45 nm synthesized with Zn_4 clusters of M(Zn_4/ZnSe) = 1/50. (d) NRs with length of ∼21 nm synthesized with Zn_4 clusters of M(Zn_4/ZnSe) = 1/30. (e) A mixture of NRs and NDs synthesized with Zn_4 clusters of M(Zn_4/ZnSe) = 1/15. (f) NDs synthesized with Zn_4 clusters of M(Zn_4/ZnSe) = 1/10. The insets present cartoons of ZnSe NCs in each case. The scale bars are 20 nm.

was applied to a TEM grid (300 mesh Cu Lacey substrate, Ted Pella, Ltd.). The excess liquid was blotted, and the specimen was vitrified by rapid plunging into liquid nitrogen using a vitrification robot system (Vitrobot Mark IV, FEI). The vitrified samples were examined at −177 °C using FEI Tecnai 12 G2 TWIN TEM operated at 120 kV and equipped with a Gatan model 626 cold stage. The images were recorded by a 4Kx4K FEI Eagle CCD camera in a low-dose mode.

High-resolution TEM (HRTEM) was performed using a FEI Tecnai F20 G2 high-resolution transmission electron microscope running at an accelerating voltage of 200 keV with a field-emission gun as an electron source. The grids for HRTEM were prepared by depositing one drop of a solution of purified nanoparticles onto an ultrathin carbon-coated grid.

Inductively coupled plasma mass spectroscopy (ICP-MS) was carried out in an Agilent 7500cx in order to correlate between the solution ratio and the actual number of impurities per NC. First, the NC samples were dried under vacuum, after which they were dissolved in a 70% HNO_3 solution (Sigma) and diluted to a final concentration of 3% HNO_3 with triply distilled water. The impurity concentration was calculated versus a calibration curve based on reference samples prepared using a 1000 ppm standard solution (High Purity Standards).

X-ray absorption fine structure (XAFS) spectroscopy measurements were taken on the ZnSe NCs synthesized with Zn_4 clusters and Cu_4 clusters. The XAFS data of ZnSe NCs synthesized with Zn_4 clusters were measured at the BL2-2 beamline at Stanford Synchrotron Radiation Lightsource (SSRL) and the XAFS data of ZnSe NCs synthesized with Cu_4 clusters were collected at 20-BM beamline at Advanced Photon Source (APS). The samples were deposited on Kapton film and sealed inside glovebox. The Zn and Se K-edge were measured in transmission mode and Cu K-edge was measured in fluorescence mode. XAFS data were processed and analyzed using the Athena and Artemis software within Demeter package.[33,34]

RESULTS AND DISCUSSION

In a typical synthesis of ZnSe NCs, NRs and NWs using our method, diethyl zinc precursor is reacted with DPP-Se in OLA and ODE initially at 60 °C generating ZnSe MSCs. The reaction solution is then heated to 240 °C for 4 h and ZnSe NWs are obtained. Adding $[Zn_4(SPh)_{10}](Me_4N)_2$ clusters at different concentration ratios prior to heating to 240 °C allows to tune the length of the NWs to generate ZnSe NRs as well as ZnSe NDs.

Figure 1 shows TEM images of ZnSe NCs with different shape and size synthesized in this manner. Without the Zn_4 clusters, ZnSe NWs with diameter of 2.4 nm and length of a few hundred nanometer are synthesized, as shown in Figure 1a. Upon addition of Zn_4 clusters, the NWs growth is disrupted leading to formation of NRs with length that can be further shortened by adding more Zn_4 clusters.

When the molar ratio of Zn_4 clusters to ZnSe precursors (M(Zn_4/ZnSe)) was 1/100, ZnSe NRs with length of 60 nm were synthesized (Figure 1b), while increased amount of Zn_4 clusters provided ZnSe NRs with length of 45 nm (Figure 1c) and 21 nm (Figure 1d) for M(Zn_4/ZnSe) = 1/50 and 1/30, respectively. Figure S1 in Supporting Information (SI) gives the histograms of the length of ZnSe NRs synthesized with different amounts of Zn_4 clusters. The ZnSe NWs and NRs manifest similar band gap absorption peak at 378 nm (Figure S2 in SI), reflecting their similar diameter of 2.4 nm.

When the molar ratio of Zn_4 clusters to ZnSe was further increased to 1/15, a mixture of ZnSe NRs and NDs was obtained (Figure 1e). This is an intermediate state between ZnSe NRs and ZnSe NDs. When we further increased the ratio of Zn_4 clusters to M(Zn_4/ZnSe) = 1/10, pure spherical ZnSe NCs (dots) with 2.3 nm diameter were observed (Figure 1f). The ZnSe NDs also show a similar absorption peak at 378 nm as that for the ZnSe NRs (Figure S2 in SI). The ZnSe NCs can therefore be tuned from NWs to NRs and even to NDs by increasing the relative amount of Zn_4 clusters.

DOI: 10.1021/jacs.8b05941
J. Am. Chem. Soc. 2018, 140, 14627−14637

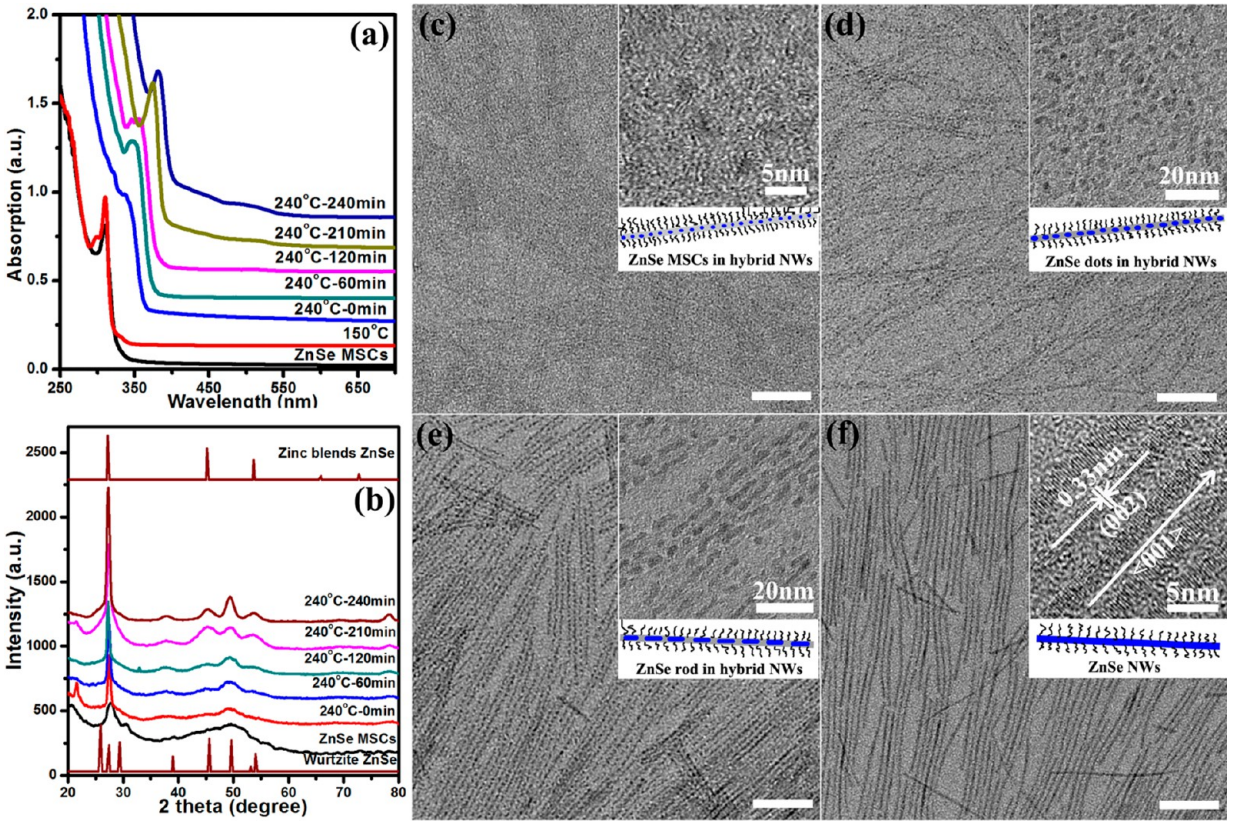

Figure 2. (a) UV−vis absorption spectra of ZnSe NCs taken at different reaction stage and time; (b) XRD patterns of ZnSe NCs taken at different reaction stage and time; (c−f) TEM images and illustrations of the NCs at different reaction stages: (c) 150 °C, ultrathin NWs with small ZnSe NDs; (d) 240 °C (0 min), hybrid NWs with separated ZnSe NDs; (e) 240 °C (210 min), hybrid NWs with separated rods; (f) 240 °C (240 min), ZnSe NWs. Scale bars are 50 nm.

Without Zn_4 clusters added in the experiment, we can get ZnSe NWs of hundreds of nanometers in length. Compared with other reports for colloidal ZnSe NWs synthesized by the attachment method, our synthesis of ZnSe NWs was performed over a longer reaction time (4 h). To follow the formation mechanism of the ZnSe NWs, aliquots were taken at different temperature and time, and characterized by UV−vis absorption spectra, powder XRD and TEM. As discussed above, the growth of ZnSe NWs started from synthesis of ZnSe MSCs at 60 °C. At the beginning of the reaction, the absorption has a sharp peak at 310 nm (Figure 2a). This corresponds to a new type of ZnSe MSCs, different from the previous reported ZnSe MSCs with absorption peaks at 307 and 322 nm.[35] Powder XRD of the ZnSe MSCs manifests broad peaks (as expected for such small particles) with positions corresponding to the wurtzite crystal structure (black line in Figure 2b), similar to the previous ZnSe NCs synthesized at low temperature.[25,35]

The solution of ZnSe MSCs in ODE and OLA was then heated to 240 °C with 15 °C/min. At 150 °C, the absorption peak at 310 nm is even more pronounced, indicating the presence of the same ZnSe MSCs as those obtained at low temperature. The TEM image (Figure 2c) manifests some ultrathin NW structures, within which individual small ZnSe MSCs are incorporated. We therefore conjecture that the ultrathin hybrid inorganic organic NWs are self-assembled via a template formed by heating ZnSe MSCs with OLA ligands to 150 °C.

Upon reaching 240 °C, ZnSe MSCs with absorption peak at 310 nm grew to two larger ZnSe MSCs with absorption peaks at 322 and 347 nm (Figure 2a), respectively. After 60 min at 240 °C, the absorption peak at 322 nm disappeared, and the absorption peak shifted to 347 nm. After 120 min at 240 °C, we observed two different absorption peaks at 347 and 355 nm indicating further growth. After 210 min at 240 °C, one peak at 355 nm remains. At the end of the reaction after 240 min at 240 °C, the absorption peak shifted to 378 nm. Figure 2 also presents TEM and HRTEM images showing the growth process of ZnSe NCs to ZnSe NWs at 240 °C. In the hybrid NWs, ZnSe MSCs not only grew to ZnSe NCs with larger diameter, they also started to attach each other forming short rods (e.g., Figure 2e). When we further heated the reaction solution at 240 °C for 240 min, these short ZnSe rods continued to elongate and connect to each other forming ZnSe NWs within the hybrid NW template.

During the formation of ZnSe NWs, the crystal structure manifested wurtzite structure as seen by powder XRD (Figure 2b). The diffraction peak from the (002) plane increased upon prolonging the reaction time at 240 °C, indicating the growth direction of ZnSe NRs is ⟨001⟩. In HRTEM images of ZnSe NWs, the (002) planes are identified, also consistent with growth along the ⟨001⟩ direction (Figure 2f).

To further establish our conjecture that hybrid NWs acted as a template in the synthesis of ZnSe NWs, cryogenic TEM was measured to probe directly the morphology in solution. Cryo-TEM is widely used to characterize soft materials providing an effective way to investigate the organic components of the hybrid NWs as well.[36−38] Figure S3 in SI presents the cryo-TEM images for aliquots taken at different reaction times at 240 °C. At 0 min at 240 °C, thin fibers with length of hundreds of

DOI: 10.1021/jacs.8b05941
J. Am. Chem. Soc. 2018, 140, 14627−14637

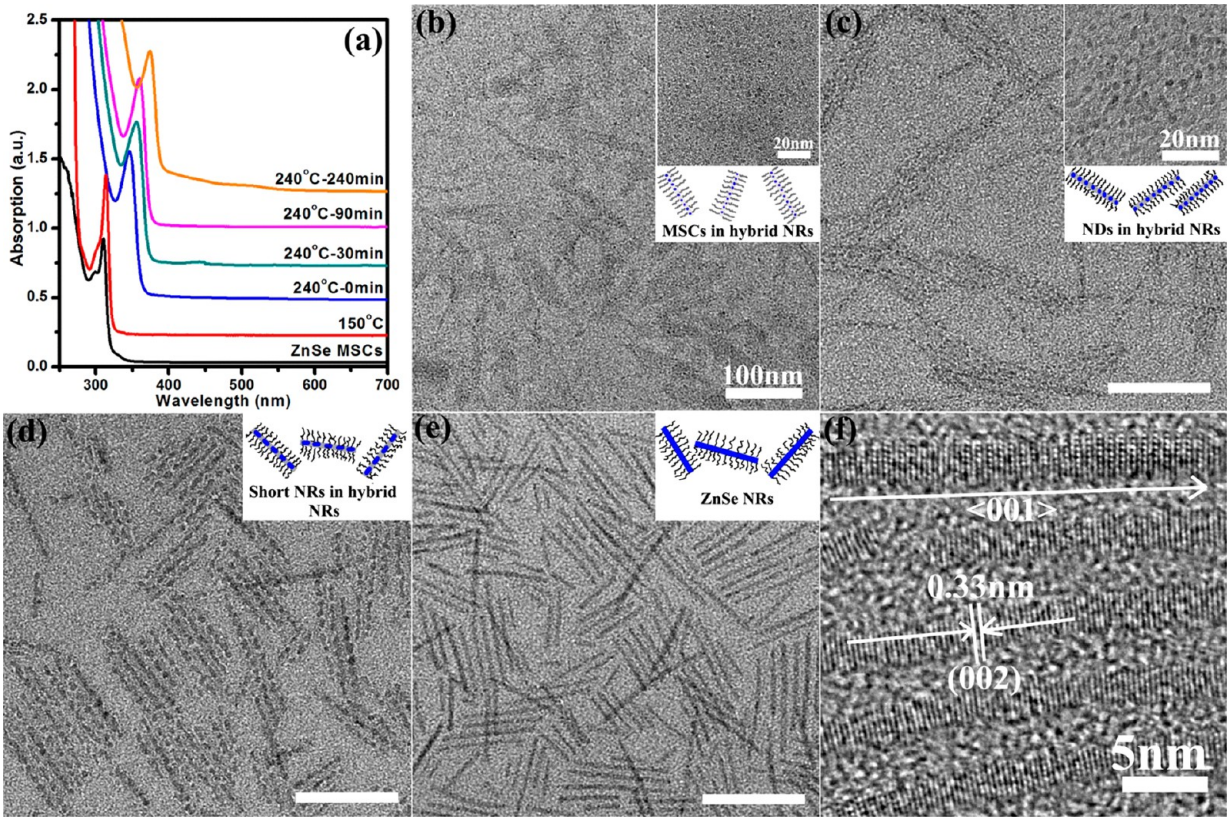

Figure 3. UV−vis absorption spectra, TEM images and HRTEM image of ZnSe NCs taken at different reaction stage and time in the synthesis of ZnSe NRs with M(Zn_4/ZnSe) = 1/50. (a) UV−vis absorption spectra of ZnSe NCs taken at different reaction stage and time. (b) Sample taken at 150 °C; short ultrathin hybrid NR template incorporating ZnSe MSCs. (c) Sample taken at 240 °C (0 min); hybrid rods with disconnected dots. (d) Sample taken at 240 °C (210 min); hybrid NRs with disconnected ZnSe NRs. (e) Sample taken at 240 °C for 240 min, ZnSe NRs are observed. (f) HRTEM image of ZnSe NRs shows the lattice of ZnSe. The ZnSe NWs grew along the ⟨001⟩ direction. The inset schemes illustrate the model of growth of ZnSe NWs at different reaction stage. The scale bar is 50 nm.

nanometers are observed, related to the hybrid NWs (Figure S3a in SI). After 120 and 210 min at 240 °C, clear NWs are observed (Figure S3b and S3c in SI, respectively). The individual ZnSe NCs could not be resolved in the cryo-TEM images, probably due to lack of contrast between the hybrid template and the ZnSe NCs in this method. Nevertheless, the contrast of the hybrid NWs increases with adding reaction time. This is attributed to the growth of the ZnSe NCs from dots to rods and finally to NWs.

These direct observations of the hybrid NWs acting as the template for ZnSe NWs, is related to other reports on growth of related II-VI semiconductor NRs and NWs based on MSCs.[39] The hybrid template played a key role in the formation of ZnSe NWs, smaller ZnSe MSCs grow to larger ones and then to short rods, and the short rods can connect to each other to form ZnSe NWs in the hybrid template. The excess monomers or dissolved smaller ZnSe NCs may provide the additional precursors to further elongate short rods to connect to each other and form ZnSe NWs within the hybrid template.

Following the mechanistic study of the NW growth discussed above, we now turn our attention to the mechanism of rod and dot formation upon adding the Zn_4 clusters. Figure 3 presents characterization of aliquots taken at different reaction stages for ZnSe NRs synthesized with M = 1/50 and used as a model to investigate the formation mechanism (see Figures S4 and S5 in SI for other ratios). The Zn_4 clusters were added to the solution of ZnSe MSCs within OLA and ODE (with absorption peak at 310 nm), and stirred at 60 °C for 4 h while maintaining the same absorption peak. While the overall behavior upon heating to 240 °C resembles that of the synthesis without the Zn_4 clusters discussed above, there are important difference. The spectral features at the absorption onset are sharper indicating a narrower diameter distribution. Significantly, short hybrid NR template structures are observed to form already at the early stages (Figure 3b,c). They are clearly resolved at 120 min at 240 °C (Figure 3d), and lead to the nanorods forming at the end of the reaction (240 min, Figure 3e,f). Moreover, we attempted to characterize this stage of thin and low contrast ZnSe NCs taken at 230 min of 240 °C via HRTEM to further investigate the formation process. As shown in HRTEM images (Figure S6 in SI), these isolated ZnSe NCs can attach in the hybrid template to form ZnSe NRs with single crystal structure.

All of the short ZnSe NRs have the diameter of 2.4 nm. This is in-line with the previous reports for ZnSe NWs or NRs synthesized with amine ligand, where the diameter of the produced NWs is mainly below 3 nm. It is difficult to get larger diameter 1D ZnSe NWs or NRs with amine ligands at 240 °C. We have therefore used a ripening process to increase the diameter of ZnSe NRs by keeping the ZnSe NRs at 280 °C for 60 min. After the high temperature ripening, the absorption peak of ZnSe NRs shifted to 405 nm and the diameter of ZnSe NRs increased to 3.6 nm as shown in the TEM images (Figure S7 in SI). Compared to ZnSe NRs before ripening, the length of the ZnSe NRs is slightly shortened. Our previous work about ZnSe NRs discussed in detail the high temperature ripening process of ZnSe NRs.[27]

DOI: 10.1021/jacs.8b05941
J. Am. Chem. Soc. 2018, 140, 14627−14637

Bulk ZnSe has wide band gap of 2.7 ev,[17] and thus its nanocrystals have the potential to serve as blue emitters. The fluorescence emission of ZnSe NRs with different diameters is presented in Figure 4. ZnSe NRs synthesized at 240 °C show a sharp emission peak at 390 nm related to the band gap recombination. An additional broad peak between 500 and 600 nm is assigned to surface trap state related emission. A quantum yield (QY) of ∼1.0% is obtained for the band gap emission, a value consistent with the organic ligand passivated rods, without the presence of an inorganic shell. After heating at 280 °C, the diameter of the ZnSe NRs increased to 3.6 nm, and correspondingly, the absorption and emission peak of ZnSe NRs have the obvious red shift because of the decreased quantum confinement effect. The broad emission peak from the surface trap emission is not seen, while only the sharp emission peak from the band gap recombination of ZnSe NRs can be observed. The QY of ZnSe NRs can reach around ∼2.0%. The increase in QY is induced by the improvement of crystallization of ZnSe and the decrease in surface defects in the high temperature process.

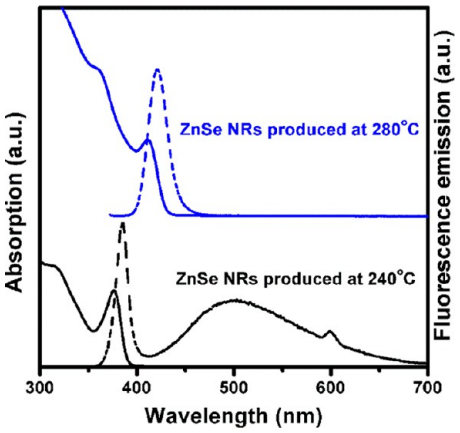

Figure 4. UV−vis absorption spectra (solid lines) and fluorescence emission (dashed lines) of ZnSe NRs synthesized at different temperatures. Shown are results for ZnSe NRs with diameter of 2.4 nm synthesized at 240 °C (black color), and for ZnSe NRs with diameter of 3.6 nm synthesized at 280 °C (blue color).

When the amount of added Zn_4 clusters is above a critical value, ZnSe NDs with uniform size distribution can be synthesized (Figure 1f). TEM images and UV−vis absorption spectra of the ZnSe NCs were taken at different reaction time with the ratio of M(Zn_4/ZnSe) = 1/10 to follow the formation of ZnSe NDs (Figure 5). ZnSe MSCs grow to bigger ZnSe NDs, and the absorption peak shows a red shift (Figure 5e). The ZnSe NDs were dispersed in the solution and continued to grow to bigger ZnSe NDs, and there was no self-assembly process to hybrid NWs during the heating process (Figure 5a−c). Further increasing the amount of Zn_4 clusters to M(Zn_4/ZnSe) = 1/5, results in a similar growth process to ZnSe NDs, as shown in Figure S8 in SI. At 240 °C, the diameter of ZnSe NDs can grow to ∼2.4 nm because of the growth limitation by the amine

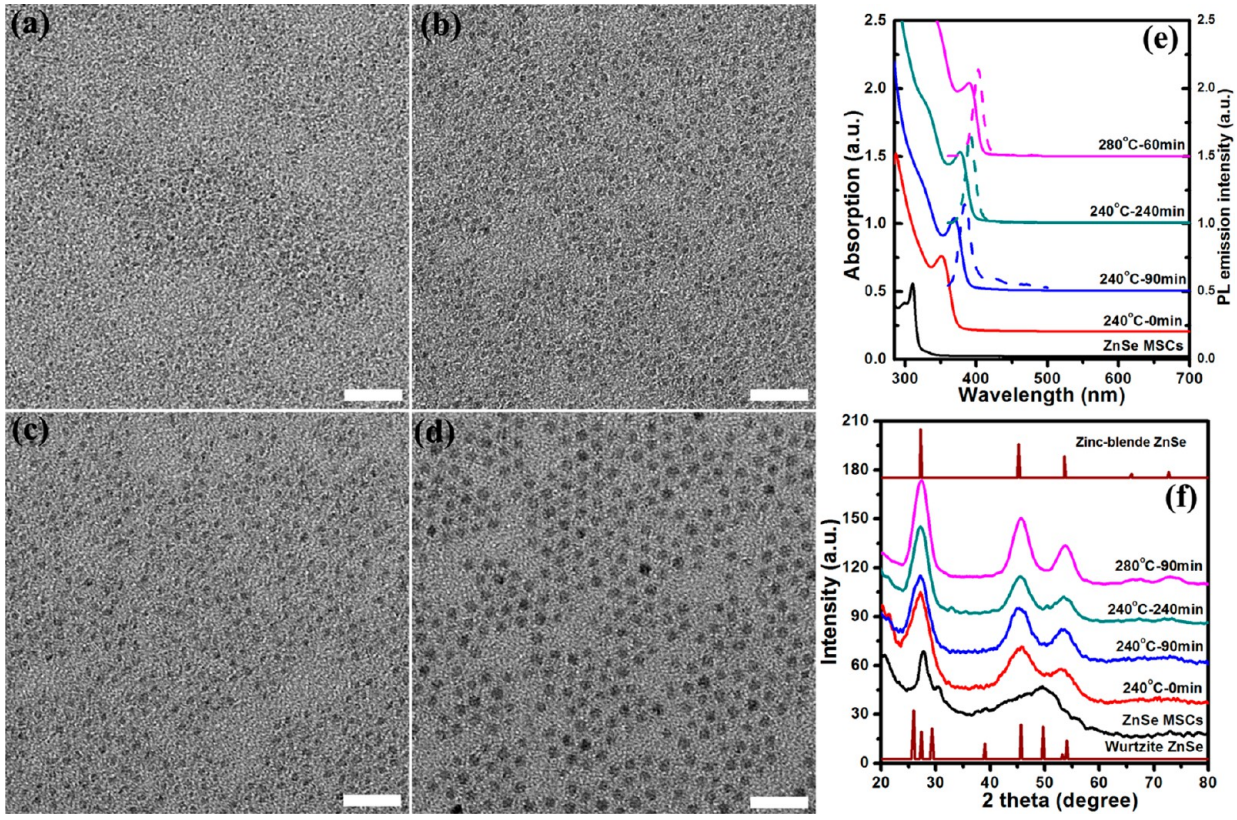

Figure 5. TEM images, UV−vis absorption spectra and XRD measurement of ZnSe NCs taken at different reaction time at 240 °C in synthesis of ZnSe NDs with M(Zn_4/ZnSe) = 1/10. (a) ZnSe NDs taken at 240 °C for 0 min. (b) ZnSe NDs taken at 240 °C for 90 min. (c) ZnSe NDs taken at 240 °C for 240 min. (d) ZnSe NDs taken at 280 °C for 60 min. (e) Absorption spectra (solid line) and fluorescence emission (dash line) of ZnSe NDs taken at different reaction time. (f) XRD patterns of ZnSe NDs taken at different reaction time. The bottom pattern shows standard diffraction peaks of wurtzite ZnSe, and the top one shows standard diffraction peaks of zinc-blende ZnSe. The scale bar is 20 nm.

DOI: 10.1021/jacs.8b05941
J. Am. Chem. Soc. 2018, 140, 14627−14637

ligands. Upon heating the ZnSe NDs to 280 °C for 1 h, they grow to 3.6 nm (Figure 5d). All of the ZnSe NDs showed a sharp fluorescence emission (Figure 5e). The full width at half-maximum intensity (fwhm) is 14 nm, indicating the high quality and homogeneous size dispersion of the ZnSe NDs. ZnSe NDs synthesized at 240 °C have a QY of ~2−3%, which increases to ~5% after the heating at 280 °C due to improved crystallization of ZnSe NCs and decreased surface trap state.

Interestingly, a crystal phase transfer from wurtzite ZnSe to zinc blende ZnSe can be observed in the growth of ZnSe NDs from ZnSe MSCs. As shown in Figure 5f, the ZnSe MSCs have the wurtzite crystal structure, and the wurtzite crystal structure transfers to zinc blende structure when the ZnSe MSCs are heated to 240 °C forming bigger ZnSe NDs. When the reaction was kept at 240 °C, the diffraction peaks became stronger and narrower, consistent with the increase in diameter of ZnSe NDs.

From the above discussion, we recognized the importance of Zn_4 clusters in controlling the shape and size of ZnSe NCs via affecting the assembly of ZnSe MSCs to hybrid template. In order to understand the role of the Zn_4 clusters in the synthesis of ZnSe NRs, we performed correlative studies of the cluster's evolution along with the NR growth at different reaction time and temperature by XAFS spectroscopy. The information contained in the X-ray absorption near edge structure (XANES) portion of the X-ray absorption coefficient describes the electronic state of the absorbing atom. Information contained in the extended XAFS (EXAFS) region describes structural and dynamic properties of the local atomic environment of the absorber. Thus, by performing analyses of XANES and EXAFS measurements at the Zn K-edge and Se K-edge regions of the absorption coefficient one can separately investigate the effects of the experimental conditions on the electronic and structural environments of Zn and Se. We performed these measurements on a series of ZnSe NCs in the course of the synthesis of the ZnSe NRs with M = 1/50. Figure S9a in SI shows that the Zn K-edge XANES spectra of ZnSe MSCs and ZnSe MSCs with Zn_4 clusters are similar to each other but different from Zn_4 clusters. The spectrum of ZnSe MSCs with Zn_4 clusters is dominated by ZnSe MSCs signal due to the small Zn_4 clusters/Zn ratio (1/50). These data can be used to evaluate the progressive increase of ZnSe crystallinity with heating time, by examining both Zn K-edge and Se K-edge data. Both Zn and Se K-edge XANES spectra of ZnSe NCs measured for longer heating times better resemble their bulk ZnSe counterparts, which are consistent with the progression observed by TEM and XRD. The EXAFS data for Zn and Se, shown in Figure S9b, 9c and 9e, 9f, respectively, report the same trend. These effects are likely caused by the growth of ZnSe NC size, as shown in Figure 3.

XANES and EXAFS data obtained in the samples of ZnSe NDs with Zn_4 clusters/ZnSe MSCs ratio of 1/10 show similar trends to those in ZnSe NCs with M = 1/50 (Figure S10 in SI). The main difference between them is that the intensity of Zn−Se and Se−Zn peaks in r-space EXAFS data is relatively lower for the larger M values, consistent with the smaller size of NDs (compared to the rods) formed for M = 1/10. The data were analyzed assuming two contributions to Zn near neighbor environment (Zn−N, originating from the surface ligands, and Zn−Se) and one contribution to Se near neighbor environment (Se−Zn). For the Zn_4 clusters, the first nearest neighbors were modeled as Zn−S pairs. Quantitative data analysis confirmed this visual observation by attributing the change in the intensity to the change in the average Zn−N and Zn−Se coordination numbers (CNs). Our results show that the CN of Zn−Se of NRs reaches 3.8 ± 0.1, while it is 3.2 ± 0.1 in NDs (Figure S11, Table S1 and S2 in SI). Correspondingly, the CN of Zn−N is smaller in ZnSe NCs with smaller M, leading to nanorods. These two trends are both consistent with larger surface to volume ratio for smaller M values (dots vs rods).

Another important observation from the EXAFS data for M = 1/10 is the absence of Zn−S signal that would have manifested as a feature at the shorter distance compared to the main Zn−Se peak in Figure S10c. For this M ratio, if all Zn_4 clusters remained intact, the 4/10th of all Zn atoms would have seen S neighbors, giving rise to their EXAFS signatures. The absence of such signatures is the evidence of Zn_4 cluster decomposition. More direct evidence of such cluster decomposition is demonstrated for Cu_4 clusters, as discussed below.

As demonstrated above, with Zn_4 clusters, we can control the template to synthesize ZnSe NCs with different shape and size. We extended this approach to other molecular clusters, specifically to $[Cu_4(SPh)_6](Me_4N)_2$ (Cu_4 clusters). With these Cu_4 clusters, isostructural to Zn_4 ones, we also obtained ZnSe NRs with length of 70−80 nm grown by a similar mechanism (Figure 6c). Inductively coupled plasma mass spectroscopy (ICP-MS) measurement for the ZnSe NRs synthesized with Cu_4 clusters showed complete incorporation of Cu into the formed ZnSe NRs.

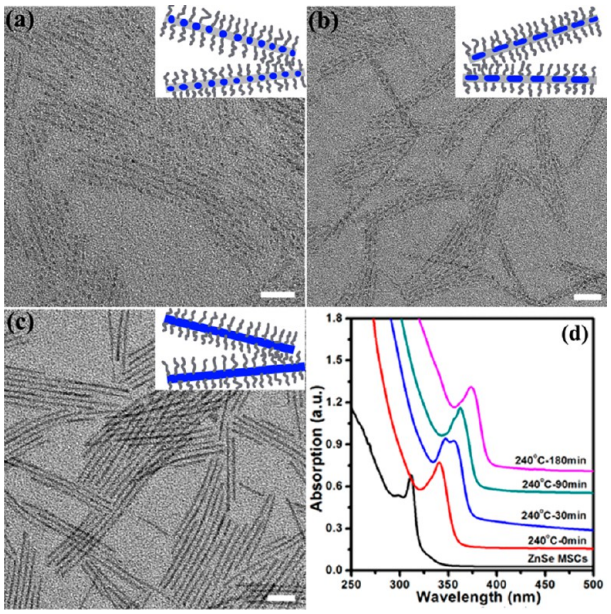

Figure 6. TEM images and UV−vis absorption spectra of ZnSe NCs taken at different reaction time at 240 °C in synthesis of ZnSe NRs with Cu_4 clusters of M(Cu_4/ZnSe) = 1/100. (a) Sample taken at 240 °C for 0 min. (b) Sample taken at 240 °C for 90 min. (c) Sample taken at 240 °C for 240 min. (d) Absorption spectra of ZnSe NCs synthesized with Cu_4 clusters taken at different reaction time. The scale bar is 20 nm.

Generally, Cu impurities can introduce the dopant energy level in the ZnSe band gap, and a new emission peak with a large red shift may be detected.[40] In the present case, indeed a new weak emission peak around 570 nm can be observed, as shown in Figure S12, which may originate from the Cu impurity.

An additional elegant attribute of the Cu_4 clusters is in its ability to help identify the role of cluster atoms separately from the majority of the host Zn atoms. Indeed, when Zn_4 clusters were used, only information on the average environment around

DOI: 10.1021/jacs.8b05941
J. Am. Chem. Soc. 2018, 140, 14627−14637

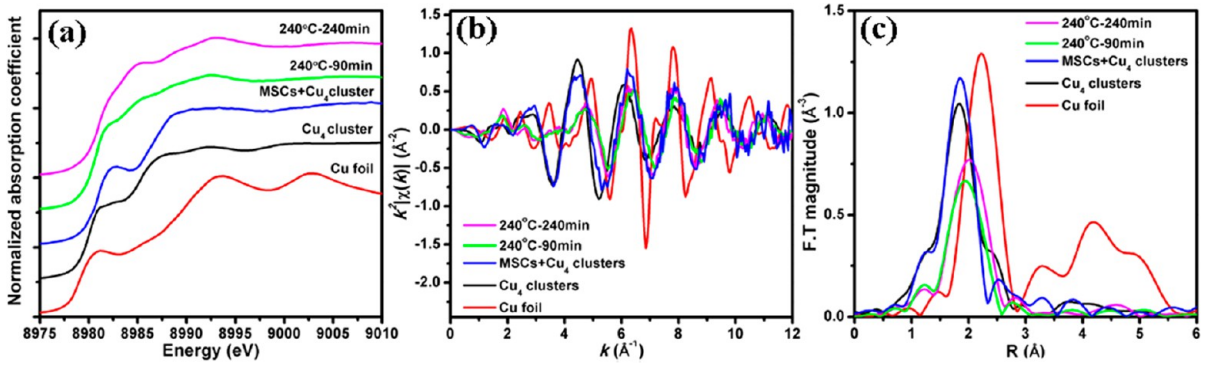

Figure 7. Cu K-edge XANES (a), k^2-weighted χ(k) (b) and Fourier transform magnitudes of k^2-weighted EXAFS (c) of ZnSe NCs synthesized with Cu_4 clusters of M(Cu_4/ZnSe) = 1/100 and with different reaction time, compared with that of bulk ZnSe and ZnSe MSCs.

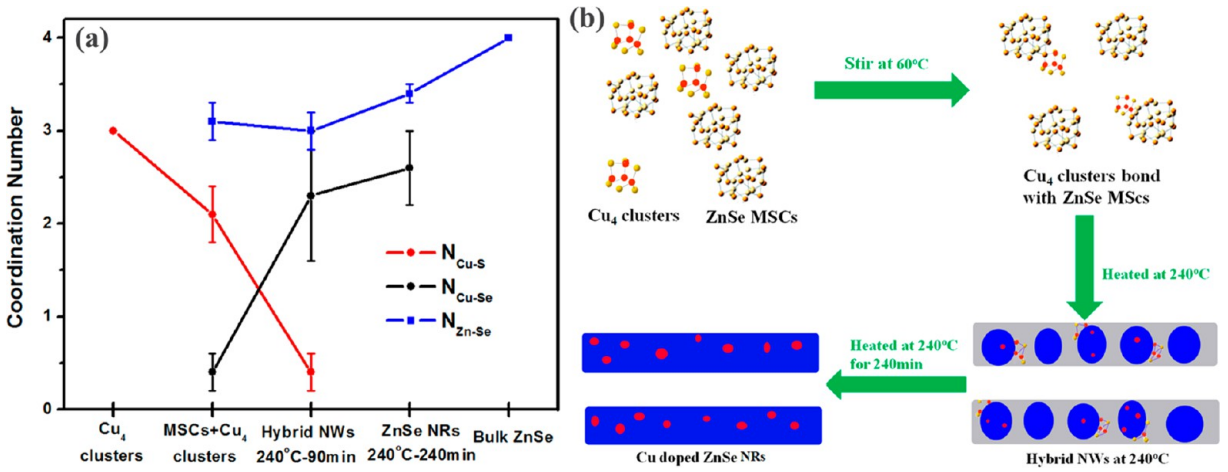

Figure 8. (a) Coordination numbers (CNs) of Cu−S, Cu−Se, and Zn−Se pairs in ZnSe NCs synthesized with M = 1/100 and with different reaction time, compared with that of Cu_4 clusters, ZnSe MSCs, and bulk ZnSe. (b) Structure model for Cu_4 clusters and ZnSe NCs at different reaction stage.

all Zn atoms (dominated by the ZnSe host) in the sample was obtained by the Zn K-edge XANES and EXAFS analyses. In the case of Cu_4 clusters, the use of the Cu K-edge XANES and EXAFS data enabled separate investigation of the cluster components contributions.

The main absorption edge region in the Cu K-edge XANES spectrum corresponds to the 1s to 4p transition, and the intensities and energy positions in the spectrum are sensitive to the geometry and local structure of the Cu atoms.[41,42] The XANES spectra (Figure 7) at the Cu K-edge show changes after Cu_4 clusters were added into ZnSe MSCs, most notably upon heating. The presence of metallic Cu was ruled out on the basis of EXAFS data analysis.

By visual observation of Fourier transform magnitudes of k^2-weighted EXAFS data at Cu K-edge (Figure 7c), we find the features in EXAFS spectra of Cu_4 clusters and Cu_4 clusters with ZnSe MSCs to be similar, but distinctly different from those in hybrid NWs and ZnSe NRs. There is a strong Cu−S peak observed in both Cu_4 clusters and Cu_4 clusters mixed with ZnSe MSCs, whereas in hybrid NWs and ZnSe NRs the major peak at longer distance is attributed to Cu−Se pairs, which is confirmed by further quantitative analysis of the EXAFS data.

As shown in Figure 8a, the CN of Cu−S decreases from 3.0 in Cu_4 clusters to 2.1 ± 0.3 in Cu_4 clusters with ZnSe MSCs and to 0.4 ± 0.2 in hybrid NWs. Meanwhile, the CN of Cu−Se increases from 0.4 ± 0.2 in the mixture with ZnSe MSCs to 2.3 ± 0.7 in hybrid NWs and 2.6 ± 0.4 in ZnSe NRs. The bond distance of Cu−Se (Table S3 in SI) decreases from 2.45 ± 0.03 Å in the mixture of ZnSe MSCs with Cu_4 clusters to about 2.36 ± 0.01 Å in hybrid NWs and 2.38 ± 0.01 Å in ZnSe NRs, which is similar to the earlier reported value (~2.34 Å) in the case of Cu internally substituting Zn in Cu^+ doped ZnSe NCs.[43] Such changes in CN and bond distances indicate the process of Cu substituting the Zn: in the beginning Cu substitutes Zn on the surface and then enters the lattice. Such substitution is reminiscent of the well reported and studied process of cation exchange in semiconductor nanocrystals.[44,45]

The size growth of ZnSe NRs may also contribute to the increasing CN of Zn−Se. Cu K-edge EXAFS results support the hypothesis that the Cu atoms enter the ZnSe NCs structure by substituting Zn atoms. The increase of CN of Zn−Se from 3 to 4 indicates the growth of ZnSe NCs, the ZnSe MSCs grow to ZnSe NRs, and surface truncation effects would correspondingly decrease with the NC size.

Figure 8 proposes the model for the evolution of Cu_4 clusters in the synthesis of Cu doped ZnSe NRs. Cu_4 clusters can bond with ZnSe MSCs at the surface after stirring the Cu_4 clusters and ZnSe MSCs at 60 °C. Weak Cu−Se binding can be observed at this stage. When the solution was heated to 240 °C, ZnSe MSCs continued to grow to larger sized ZnSe NCs, and the Cu_4 clusters started to be embedded into ZnSe NCs during the growth of ZnSe MSCs. Cu_4 clusters decomposed to Cu ions, and these Cu ions diffused into ZnSe to form dopants, as demonstrated by the decrease in the Cu−S CN and the

DOI: 10.1021/jacs.8b05941
J. Am. Chem. Soc. 2018, 140, 14627−14637

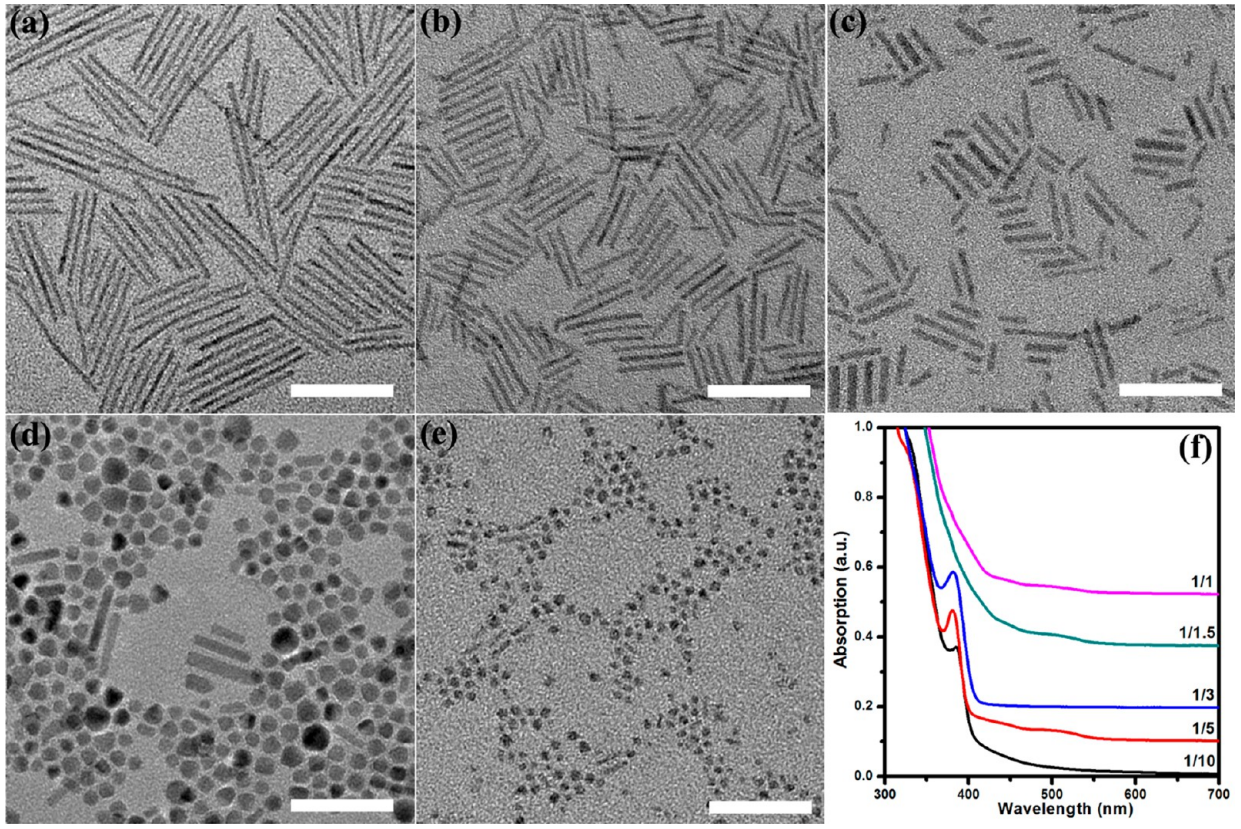

Figure 9. TEM images and UV−vis absorption spectra of ZnSe NCs synthesized with different amount of thiophenol in the reaction. (a) ZnSe NRs (65 nm) synthesized with thiophenol of M(SPh/ZnSe) = 1/10, which are according to Zn_4 clusters of M(Zn_4/ZnSe) = 1/100. (b) ZnSe NRs (35 nm) synthesized with thiophenol of M(SPh/ZnSe) = 1/5, which are according to Zn_4 clusters of M(Zn_4/ZnSe) = 1/50. (c) ZnSe NRs (25 nm) synthesized with thiophenol of M(SPh/ZnSe) = 1/3, which are according to Zn_4 clusters of 1/30 of M(Zn_4/ZnSe). (d) The mixture of NRs and NDs synthesized with thiophenol of M(SPh/ZnSe) = 1/1.5, which are according to Zn_4 clusters of M(Zn_4/ZnSe) = 1/15. (e) ZnSe NDs synthesized with thiophenol of M(SPh/ZnSe) = 1/1, which are according to Zn_4 clusters of M(Zn_4/ZnSe) = 1/10. (f) Absorption spectra of ZnSe NRs synthesized with different ratio of thiophenol to ZnSe as noted. The scale bar is 50 nm.

concomitant increase in the Cu−Se CN. In the end, only Cu−Se bonding can be seen in ZnSe NRs as Cu_4 clusters completely decomposed to Cu ions and formed Cu dopants in ZnSe NRs.

The behavior of the Zn and Se K-edge spectra in the presence of Cu_4 clusters (Figure S13 in SI) resembles the results obtained for the Zn_4 clusters described above. Fitting results (Figure 8) confirm the qualitative trends and are consistent with those obtained for the Zn_4 clusters. This similarity is expected because of the relatively small ratios of Cu to Zn atoms in ZnSe in this experiment.

The above analysis proves that the Cu_4 clusters decompose and are incorporated into the ZnSe. Similar evidence was obtained for Zn_4 clusters at high M values, as shown above. It is still important to understand how did the Zn_4 clusters and Cu_4 clusters affect the self-assembly of ZnSe MSCs to form the hybrid NWs? Both isostructured Zn_4 and Cu_4 clusters have the same ligands, thiophenol, and to isolate the role of the ligands, experiments while adding thiophenol instead of clusters in the synthesis, were performed. The amounts of added thiophenol corresponded to those in the synthesis using Zn_4 clusters. Figure 9 presents TEM images of ZnSe NCs produced with different amount of thiophenol. The ZnSe NCs can be tuned from rods to dots upon increasing the amount of thiophenol in the experiment. With thiophenol amount analogous to M = 1/10, ZnSe NRs with length of 65 nm were obtained (Figure 9a).

The formation mechanism of ZnSe NRs produced with thiophenol was investigated as shown in Figure S14, providing a similar formation mechanism to that of ZnSe NRs synthesized with Zn_4 clusters. With some thiophenol in the reaction, ZnSe MSCs can self-assemble to short hybrid rods. Based on these short hybrid rods acting as template, ZnSe MSCs can grow to bigger dots and short rods. In the end, these can fuse to form ZnSe NRs.

Increasing the amount of added thiophenol leads to shortening of the length of the ZnSe NRs, and can lead also to formation of ZnSe NDs. When we further increased the amount of thiophenol to M(SPh/ZnSe) = 1/1.5 in the reaction, a mixture of rods and dots was produced, in correspondence to Zn_4 clusters of M(Zn_4/ZnSe) = 1/15 (Figure 9d). This is an intermediate state between rods and dots. Pure ZnSe NDs were produced when the amount of thiophenol was M(SPh/ZnSe) = 1/1 (Figure 9e). However, the size distribution of the ZnSe NDs is broad, unlike the ZnSe NDs produced with Zn_4 clusters, and the absorption spectra of ZnSe NDs manifests only a broad shoulder (Figure 9f).

Therefore, the reaction using Zn_4 clusters provides better control over the size and shape distribution of the ZnSe rods and dots. The difference may be that Zn_4 clusters provide thiophenol to control the self-assembly of the hybrid template, while also supplying additional Zn precursor for the synthesis of ZnSe NCs. Furthermore, their release from the clusters is likely gradual evidently helping in synthesis of high quality ZnSe NCs in the reaction.

DOI: 10.1021/jacs.8b05941
J. Am. Chem. Soc. 2018, 140, 14627−14637

In the self-assembly of ZnSe NCs to hybrid nanostructures, the OLA ligand played an important role. However, upon addition of some Zn_4 clusters or thiophenol in the reaction, the self-assembly process can be altered. With molecular clusters, we can control the self-assembly of ZnSe NCs to hybrid template with different length. Based on different hybrid templates, ZnSe NCs with different shape and size can be synthesized. In the reaction, the molecular clusters and the thiophenol limit the formation of the hybrid template in controlled manner. By this, the length of hybrid NWs would become shorter and shorter via increasing the amount of molecular clusters in the reaction. When the amount of molecular clusters is sufficiently large, ZnSe NCs do not self-assemble to hybrid nanostructures, and individual ZnSe NDs can be produced. When using thiophenol instead of clusters, a similar trend is seen, but with significantly broader size and shape distribution.

CONCLUSION

ZnSe NCs, including ZnSe NWs, NRs and NDs, can be synthesized in controlled manner via adding Zn_4 molecular clusters in the reaction. A new ZnSe MSCs with absorption peak at 310 nm can be synthesized at 60 °C, and these ZnSe MSCs can self-assemble to hybrid NWs during the heating process. Based on this hybrid NW template, ZnSe NWs can be synthesized. The hybrid NWs act as template for formation of the final ZnSe NCs. When we add Zn_4 clusters in the reaction, they can change the hybrid template to get differently shaped and sized ZnSe NCs. The experiment can be extended to other molecular clusters, such as Cu_4 clusters. The Cu_4 clusters also can act as marker atoms to investigate the changes of the molecular clusters during the synthesis of the ZnSe NCs. In the formation of ZnSe NRs with Cu_4 clusters, the entire Cu element was incorporated into the ZnSe NRs to form dopants.

The ligand of the molecular clusters, thiophenol, plays an important role in the self-assembly of ZnSe MSCs to form hybrid elongated structures. Thiophenol can be used instead of molecular clusters to synthesize ZnSe NCs, by a similar formation mechanism. The thiophenol ligand can prevent the self-assembly of ZnSe NCs with amine ligand to form hybrid NWs. The hybrid NWs become shorter and shorter, and then disappear via increasing the amount of clusters or thiophenol in the reaction. Compared to synthesis of ZnSe NCs produced with thiophenol only, Zn_4 clusters can also provide additional zinc precursor to ZnSe NCs, which offers an optimal approach to synthesize high quality and homogeneous ZnSe NCs.

This template controlled approach can be extended to other semiconductor NCs system to tune the shape and size. For example, ZnS NWs, NRs and NDs could be produced by using DPP-S instead of DPP-Se. As exemplified by use of the Cu_4 clusters, other molecular clusters can be used offering an approach for doping the NCs during the synthesis. Other amine ligands can also be used to control the hybrid template. All this provides a broad tool set for synthesis of well controlled rods and dots of additional semiconductors.

ASSOCIATED CONTENT

Supporting Information

The Supporting Information is available free of charge on the ACS Publications website at DOI: 10.1021/jacs.8b05941.

Histograms of length of ZnSe NRs synthesized with different Zn_4 clusters; absorption spectra of ZnSe NCs synthesized with different amount of Zn_4 clusters at 240 °C; cryo-TEM images of hybrid NWs taken at 240 °C at different reaction time; TEM images of ZnSe NCs taken at different reaction time at 240 °C in synthesis of ZnSe NRs with Zn_4 clusters of $M(Zn_4/ZnSe)$ = 1/100 and 1/30; HRTEM images of ZnSe NCs taken at 230 min of 240 °C in the synthesis of ZnSe NRs with Zn_4 clusters of $M(Zn_4/ZnSe)$ = 1/50; absorption spectra and TEM images of ZnSe NRs repining at 280 °C for 60 min based on ZnSe NRs with different amount of Zn_4 cluster; TEM images and absorption spectra of ZnSe NDs synthesized with Zn_4 clusters of $M(Zn_4/ZnSe)$ = 1/5; Zn and Se K-edge XANES, k^2-weighted $\chi(k)$, Fourier transform magnitudes of k^2-weighted EXAFS data of ZnSe NCs synthesized with Zn_4 clusters of $M(Zn_4/ZnSe)$ = 1/50 and with different reaction time; Zn and Se K-edge XANES, k^2-weighted $\chi(k)$, Fourier transform magnitudes of k^2-weighted EXAFS data of ZnSe NCs synthesized with Zn_4 clusters of $M(Zn_4/ZnSe)$ = 1/10 and with different reaction time; coordination numbers of Zn−N, Zn−Se and Se−Zn pairs from fit results of ZnSe NCs synthesized with Zn_4 clusters of $M(Zn_4/ZnSe)$ = 1/10 and 1/50 and with different reaction time; UV−vis absorption and fluorescence emission spectra of Cu doped ZnSe NRs synthesized at 240 °C; Zn and Se K-edge XANES, k^2-weighted $\chi(k)$, Fourier transform magnitudes of k^2-weighted EXAFS and coordination Number of Zn−N, Zn−Se and Zn−Se_2 pairs data of ZnSe NCs synthesized with Cu_4 clusters of $M(Cu_4/ZnSe)$ = 1/100; TEM images and absorption spectra of ZnSe NCs taken at different reaction time with thiophenol of $M(SPh/ZnSe)$ = 1/5, according to the amount of Zn_4 clusters of $M(Zn_4/ZnSe)$ = 1/50; Tables for fitting results of Zn K-edge EXAFS data of Zn_4 clusters-ZnSe, Se K-edge EXAFS data of Zn_4 clusters-ZnSe, Cu K-edge EXAFS data of Cu_4 clusters-ZnSe, Zn K-edge EXAFS data of Cu_4−ZnSe, and Se K-edge EXAFS data of Cu_4−ZnSe (PDF)

AUTHOR INFORMATION

Corresponding Authors

*anatoly.frenkel@stonybrook.edu
*uri.banin@mail.huji.ac.il

ORCID

Jiajia Ning: 0000-0002-7922-5469
Anatoly I. Frenkel: 0000-0002-5451-1207
Uri Banin: 0000-0003-1698-2128

Notes

The authors declare no competing financial interest.

ACKNOWLEDGMENTS

We thank Dr. Vladimir Uvarov for assistance in XRD measurement. J.N. acknowledges the support from the Planning and Budgeting Committee of the higher board of education in Israel through a fellowship. U.B. acknowledges the support of the Alfred and Erica Larisch chair. We acknowledge support of this work by NSF Grant No. CHE-1719534 and BSF Grant No. 2013/610. Use of the Stanford Synchrotron Radiation Lightsource, SLAC National Accelerator Laboratory, is supported by the U.S. Department of Energy, Office of Science, Office of Basic Energy Sciences under Contract No. DE-AC02-76SF00515. This research used resources of the Advanced Photon Source, a U.S. Department of Energy (DOE) Office of Science User Facility operated for the DOE Office of Science by Argonne

DOI: 10.1021/jacs.8b05941
J. Am. Chem. Soc. 2018, 140, 14627−14637

National Laboratory under Contract No. DE-AC02-06CH11357.

REFERENCES

(1) Kovalenko, M. V.; Manna, L.; Cabot, A.; Hens, Z.; Talapin, D. V.; Kagan, C. R.; Klimov, V. I.; Rogach, A. L.; Reiss, P.; Milliron, D. J.; Guyot-Sionnnest, P.; Konstantatos, G.; Parak, W. J.; Hyeon, T.; Korgel, B. A.; Murray, C. B.; Heiss, W. *ACS Nano* **2015**, *9*, 1012−1057.
(2) Chen, O.; Zhao, J.; Chauhan, V. P.; Cui, J.; Wong, C.; Harris, D. K.; Wei, H.; Han, H. S.; Fukumura, D.; Jain, R. K.; Bawendi, M. G. *Nat. Mater.* **2013**, *12*, 445−451.
(3) Hu, J. T.; Li, L. S.; Yang, W. D.; Manna, L.; Wang, L. W.; Alivisatos, A. P. *Science* **2001**, *292*, 2060−2063.
(4) Sitt, A.; Salant, A.; Menagen, G.; Banin, U. *Nano Lett.* **2011**, *11*, 2054−2060.
(5) Cunningham, P. D.; Souza, J. B.; Fedin, I.; She, C. X.; Lee, B.; Talapin, D. V. *ACS Nano* **2016**, *10*, 5769−5781.
(6) Protesescu, L.; Yakunin, S.; Kumar, S.; Bar, J.; Bertolotti, F.; Masciocchi, N.; Guagliardi, A.; Grotevent, M.; Shorubalko, I.; Bodnarchuk, M. I.; Shih, C. J.; Kovalenko, M. V. *ACS Nano* **2017**, *11*, 3119−3134.
(7) Panfil, Y. E.; Oded, M.; Banin, U. *Angew. Chem., Int. Ed.* **2018**, *57*, 4274−4295.
(8) Bruchez, M., Jr.; Moronne, M.; Gin, P.; Weiss, S.; Alivisatos, A. P. *Science* **1998**, *281*, 2013−2016.
(9) Bareket, L.; Waiskopf, N.; Rand, D.; Lubin, G.; David-Pur, M.; Ben-Dov, J.; Roy, S.; Eleftheriou, C.; Sernagor, E.; Cheshnovsky, O.; Banin, U.; Hanein, Y. *Nano Lett.* **2014**, *14*, 6685−6692.
(10) Keuleyan, S.; Lhuillier, E.; Guyot-Sionnest, P. *J. Am. Chem. Soc.* **2011**, *133*, 16422−16424.
(11) Lhuillier, E.; Keuleyan, S.; Liu, H.; Guyot-Sionnest, P. *Chem. Mater.* **2013**, *25*, 1272−1282.
(12) Peng, X. G.; Wickham, J.; Alivisatos, A. P. *J. Am. Chem. Soc.* **1998**, *120*, 5343−5344.
(13) Peng, Z. A.; Peng, X. G. *J. Am. Chem. Soc.* **2001**, *123*, 1389−1395.
(14) Ithurria, S.; Dubertret, B. *J. Am. Chem. Soc.* **2008**, *130*, 16504−16505.
(15) Milliron, D. J.; Hughes, S. M.; Cui, Y.; Manna, L.; Li, J. B.; Wang, L. W.; Alivisatos, A. P. *Nature* **2004**, *430*, 190−195.
(16) Deka, S.; Miszta, K.; Dorfs, D.; Genovese, A.; Bertoni, G.; Manna, L. *Nano Lett.* **2010**, *10*, 3770−3776.
(17) Hines, M. A.; Guyot-Sionnest, P. *J. Phys. Chem. B* **1998**, *102*, 3655−3657.
(18) Wang, A. Q.; Shen, H. B.; Zang, S. P.; Lin, Q. L.; Wang, H. Z.; Qian, L.; Niu, J. Z.; Li, L. S. *Nanoscale* **2015**, *7*, 2951−2959.
(19) Fang, Z.; Li, Y.; Zhang, H.; Zhong, X. H.; Zhu, L. Y. *J. Phys. Chem. C* **2009**, *113*, 14145−14150.
(20) Norris, D. J.; Yao, N.; Charnock, F. T.; Kennedy, T. A. *Nano Lett.* **2001**, *1*, 3−7.
(21) Peng, X. G.; Manna, L.; Yang, W. D.; Wickham, J.; Scher, E.; Kadavanich, A.; Alivisatos, A. P. *Nature* **2000**, *404*, 59−61.
(22) Schliehe, C.; Juarez, B. H.; Pelletier, M.; Jander, S.; Greshnykh, D.; Nagel, M.; Meyer, A.; Foerster, S.; Kornowski, A.; Klinke, C.; Weller, H. *Science* **2010**, *329*, 550−553.
(23) Panda, A. B.; Acharya, S.; Efrima, S. *Adv. Mater.* **2005**, *17*, 2471−2474.
(24) Chin, P. T. K.; Stouwdam, J. W.; Janssen, R. A. J. *Nano Lett.* **2009**, *9*, 745−750.
(25) Panda, A. B.; Acharya, S.; Efrima, S.; Golan, Y. *Langmuir* **2007**, *23*, 765−770.
(26) Sarkar, S.; Acharya, S.; Chakraborty, A.; Pradhan, N. *J. Phys. Chem. Lett.* **2013**, *4*, 3292−3297.
(27) Jia, G. H.; Sitt, A.; Hitin, G. B.; Hadar, I.; Bekenstein, Y.; Amit, Y.; Popov, I.; Banin, U. *Nat. Mater.* **2014**, *13*, 301−307.
(28) Jia, G. H.; Banin, U. *J. Am. Chem. Soc.* **2014**, *136*, 11121−11127.
(29) Acharya, S.; Sarkar, S.; Pradhan, N. *J. Phys. Chem. C* **2013**, *117*, 6006−6012.
(30) Dance, I. G.; Choy, A.; Scudder, M. L. *J. Am. Chem. Soc.* **1984**, *106*, 6285−6295.
(31) Meulenberg, R. W.; van Buuren, T.; Hanif, K. M.; Willey, T. M.; Strouse, G. F.; Terminello, L. J. *Nano Lett.* **2004**, *4*, 2277−2285.
(32) Jawaid, A. M.; Chattopadhyay, S.; Wink, D. J.; Page, L. E.; Snee, P. T. *ACS Nano* **2013**, *7*, 3190−3197.
(33) Ravel, B.; Newville, M. *J. Synchrotron Radiat.* **2005**, *12*, 537−541.
(34) Newville, M. *J. Synchrotron Radiat.* **2001**, *8*, 322−324.
(35) Zhang, L. J.; Shen, X. C.; Liang, H.; Yao, J. T. *J. Phys. Chem. C* **2010**, *114*, 21921−21927.
(36) Levi-Kalisman, Y.; Jadzinsky, P. D.; Kalisman, N.; Tsunoyama, H.; Tsukuda, T.; Bushnell, B.; Kornberg, R. D. *J. Am. Chem. Soc.* **2011**, *133*, 2976−2982.
(37) Cui, H.; Hodgdon, T. K.; Kaler, E. W.; Abezgauz, L.; Danino, D.; Lubovsky, M.; Talmon, Y.; Pochan, D. J. *Soft Matter* **2007**, *3* (8), 945−955.
(38) Newcomb, C. J.; Moyer, T. J.; Lee, S. S.; Stupp, S. I. *Curr. Opin. Colloid Interface Sci.* **2012**, *17* (6), 350−359.
(39) Wang, F. D.; Wang, Y. Y.; Liu, Y. H.; Morrison, P. J.; Loomis, R. A.; Buhro, W. E. *Acc. Chem. Res.* **2015**, *48*, 13−21.
(40) Cooper, J. K.; Gul, S.; Lindley, S. A.; Yano, J.; Zhang, J. Z. *ACS Appl. Mater. Interfaces* **2015**, *7*, 10055−10066.
(41) Kau, L. S.; Spira-Solomon, D. J.; Penner-Hahn, J. E.; Hodgson, K. O.; Solomon, E. I. *J. Am. Chem. Soc.* **1987**, *109*, 6433−6442.
(42) Shadle, S. E.; Penner-Hahn, J. E.; Schugar, H. J.; Hedman, B.; Hodgson, K. O.; Solomon, E. I. *J. Am. Chem. Soc.* **1993**, *115*, 767−776.
(43) Gul, S.; Cooper, J. K.; Glans, P.-A.; Guo, J.; Yachandra, V. K.; Yano, J.; Zhang, J. Z. *ACS Nano* **2013**, *7*, 8680−8692.
(44) Son, D. H.; Hughes, S. M.; Yin, Y. D.; Alivisatos, A. P. *Science* **2004**, *306*, 1009−1012.
(45) De Trizio, L. D.; Manna, L. *Chem. Rev.* **2016**, *116*, 10852−10887.

DOI: 10.1021/jacs.8b05941
J. Am. Chem. Soc. 2018, 140, 14627−14637